Polarizabilities of Adsorbed and Assembled Molecules: Measuring the Conductance through Buried Contacts

Amanda M. Moore,[†] Sina Yeganeh,[‡] Yuxing Yao,[§] Shelley A. Claridge,[⊥] James M. Tour,[§,*] Mark A. Ratner,[‡,*] and Paul S. Weiss[†,⊥,*]

[†]Departments of Chemistry and Physics, The Pennsylvania State University, University Park, Pennsylvania 16802, United States, [‡]Department of Chemistry, Northwestern University, Evanston, Illinois 60208-3113, United States, [§]Department of Chemistry and Smalley Institute for Nanoscale Science and Technology, Rice University, Houston, Texas 77005, United States, and [⊥]California NanoSystems Institute and Departments of Chemistry & Biochemistry and Materials Science & Engineering, University of California, Los Angeles, Los Angeles, California 90095, United States

ABSTRACT We have measured the polarizabilities of four families of molecules adsorbed to Au{111} surfaces, with structures ranging from fully saturated to fully conjugated, including single-molecule switches. Measured polarizabilities increase with increasing length and conjugation in the adsorbed molecules and are consistent with theoretical calculations. For single-molecule switches, the polarizability reflects the difference in substrate—molecule electronic coupling in the ON and OFF conductance states. Calculations suggest that the switch between the two conductance states is correlated with an oxidation state change in a nitro functional group in the switch molecules.

*Address correspondence to
tour@rice.edu,
ratner@chem.northwestern.edu,
psw@cnsi.ucla.edu.

Scientific understanding is increasingly derived from studies of single-molecule physical properties and interactions. As such measurements become more robust, single-molecule metrology tools are being dramatically enhanced by combining additional signals providing further chemical, physical, and electronic information.[1−8] For instance, single-molecule fluorescent labeling can be performed with fluorophores sensitive to specific environmental conditions[9] or using optics with anisotropic point-spread functions that can be analyzed to localize position in a third dimension.[10] Scanning probe topographic measurements can be performed with a functionalized atomic force microscope (AFM) tip that simultaneously provides both topographic and chemical information based on changes in cantilever resonance.[11]

Here, we have used the microwave frequency alternating current scanning tunneling microscope (ACSTM)[1,2,4,5,12] to image the topography and polarizability of single molecules simultaneously. Standard STM topography measurements are per-formed with a constant DC bias applied to the tip. Previously, we have reported that a microwave frequency generator can be used to modulate the DC bias in the STM, a capability that enables imaging on semiconducting and insulating surfaces by measuring tunneling both to and from the surface.

Polarizable molecules have a "soft" electron cloud that deforms in response to the high-frequency bias modulation, in turn modulating the tunneling current. Thus, the magnitude of the transmitted microwave frequency modulation correlates with the polarizability of the molecule in the tunneling junction. Since the microwave frequency modulation (GHz) is fast relative to the feedback loop (1 kHz), polarizability can be collected simultaneously with standard molecular topography images. Although polarizability is also known to contribute to topographic imaging,[13,14] here we are able to deconvolve the two components. Using this technique, we have imaged a variety of families of self-assembled monolayers (SAMs), compared relative experimental and calculated polarizabilities for each molecule, and used these measurements to study single-molecule switches.

Measurements made on surfaces have fundamental differences from those performed in the gas phase, which are important in the context of molecular devices. Gas-phase molecular polarizabilities reflect the dispersion forces within and between molecules. On surfaces, the measured electronic response also includes substrate electrons to the extent that these are coupled into the molecules. Such coupling is integral to the electronic behavior of the molecule

TABLE 1. Calculated Polarizabilities (α) of Adsorbed Molecules in Atomic Units (Bohr³) Using Density Functional Theory As Described in the Text[a]

| molecule	α	$\alpha_{molecule}/\alpha_{C12}$
octanethiol (**C8**)		
normal	158	
tilted 30°	143	0.76
dodecanethiol (**C12**)		
normal	199	
tilted 30°	189	1.00
1ATC9		
normal	241	1.28
tilted 18°	232	1.23
OPE		
normal	810	4.29
tilted 30°	643	3.40
tilted 45°	475	2.51
nitro OPE		
(neut, neut geom.)		
normal	871	4.61
tilted 30°	690	3.65
tilted 45°	508	2.69
(neut, anion geom.)		
normal	918	4.86
tilted 30°	725	3.84
tilted 45°	531	2.81
(anion, neut geom.)		
normal	1289	6.82
tilted 30°	1005	5.32
tilted 45°	722	3.82
(anion, anion geom.)		
normal	1127	5.96
tilted 30°	882	4.67
tilted 45°	639	3.38

[a]Calculations are performed for molecules in the gas phase, with no explicit contribution from substrate atoms. Values are normalized to the polarizability of dodecanethiolate tilted at 30° relative to the surface normal. Polarizabilities for tilted configurations are calculated along the axis of the applied field, assumed to be the same as the surface normal. Extending these calculations to consider the molecular polarizability within the monolayer and contributions from electrode atoms will modify these numbers somewhat.[20]

and is known to vary with both the orientation of the molecule and the substrate topography.[8,15−18] The measurements described here are uniquely able to analyze the relationship between polarizability and these other physical factors.

RESULTS AND DISCUSSION

For comparison to experiment, molecular polarizabilities were calculated using density functional theory (DFT) with the B3LYP functional and a 6-31^{++}G** basis set (Table 1).[19] These include calculations for molecules aligned normal to the surface and in tilted conformations and for both anionic and neutral states of the nitro-functionalized oligo(phenylene ethynylene) (**OPE**) molecules (Figure 1A, bottom). While we have shown that we do not need to oxidize nor reduce the molecules directly in order to cause switching (an applied electric field without current flow is sufficient),[15,17] it is
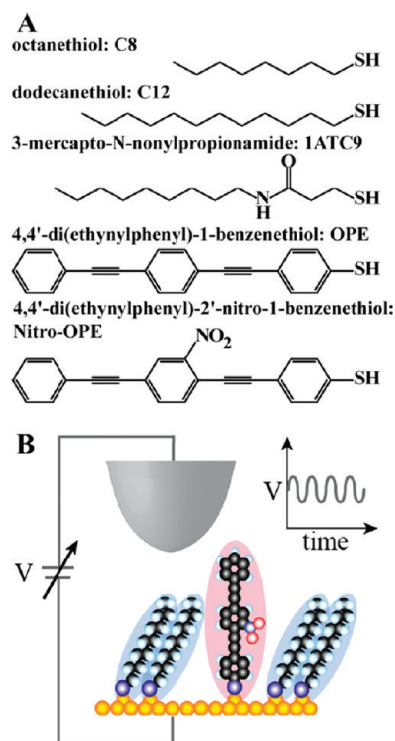

Figure 1. (A) Structures of molecules used in this study. (B) Schematic of the AC scanning tunneling microscope tip−sample junction containing self-assembled molecules of a C12 host SAM with a single switch molecule inserted at a defect site in the SAM. Microwave frequency bias modulations are applied from the STM tip and are used to measure the polarizabilities of the molecules in the junction.

possible that the ground states of molecules in different tilt conformations have different oxidation states.

We probed the polarizabilities of the molecules shown in Figure 1A by forming SAMs of octanethiolate (**C8**), dodecanethiolate (**C12**), 3-mercapto-*N*-nonylpropionamide (**1ATC9**), and unfunctionalized **OPE** molecules (4,4′-di(ethynylphenyl)-1-benzenethiol). We further related the polarizability to conductance switching by inserting single nitro-functionalized **OPE** switch molecules (4,4′-di(ethynylphenyl)-2′-nitro-1-benzenethiol) into host **C12** SAMs. Figure 1B shows a schematic of this insertion with a single-molecule switch bound in a defect site of a host **C12** SAM on Au{111} within the ACSTM tunneling junction.

Devices based on electronic switches are central to modern information technology. As miniaturization of such devices continues, nanostructures and single molecules that exhibit conductance switching must be understood and controlled within their physical environment.[21] To accomplish this, we must have the capabilities to address single switch molecules in both their ON and OFF conductance states, to predict when each molecule will be active as a switch, and to control their switching. By applying ACSTM imaging to systems of isolated **OPE** switch molecules, we are able to locate and to predict which molecules are likely to be active either through switching or through increased
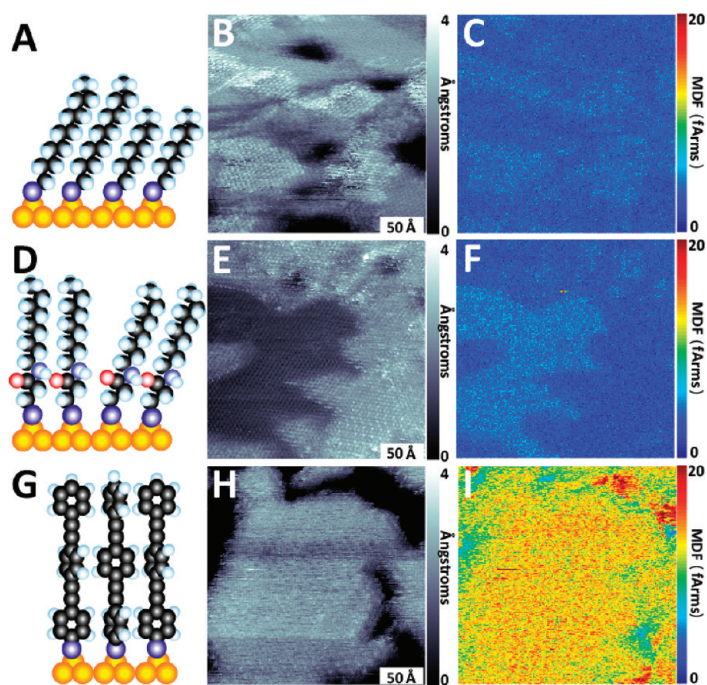
Figure 2. (A) Schematic, (B) topographic image, and (C) simultaneously recorded microwave difference frequency (MDF) image of an artificially separated self-assembled monolayer (SAM) containing dodecanethiolate (**C12**) and octanethiolate (**C8**) (see text). The topographically more protruding **C12** molecules have a larger MDF signal. (D) Schematic and (E) topographic image of a **1ATC9** SAM. Molecules with buried amide functionalities assemble with varied tilts from normal to 18° from surface normal to enable hydrogen bonding.[42] (F) Microwave difference frequency image for a **1ATC9** SAM. Note that the topographically less protruding **1ATC9** molecules have a larger MDF signal. (G) Schematic of an **OPE** SAM with structure based on the model proposed by Liu and co-workers who have measured a tilt of less than 5° for the molecules in this monolayer.[43] (H) Topographic image and (I) MDF image of an **OPE** SAM. This molecule has a larger polarizability than the alkanethiolate and amide-containing molecules, and thus we observe a larger MDF signal. Imaging conditions: V_{sample} = +1.0 V, I_{tunnel} = 1.0 pA, applied frequency = 2 GHz, difference frequency = 5 kHz, nominal input power level = 10 dBm.

motion.[22] We can switch the conductance states of single molecules while simultaneously mapping the microwave difference frequency (MDF) signal to confirm the location of each switch (even when it is not visible in conventional STM topography) and to determine differences in the molecule—substrate coupling due to bonding and structural changes.

A number of techniques have been used to study fully conjugated **OPE** molecules for use as molecular wires and molecular switches.[7,15−18,21−31] When single **OPE** molecules are isolated within host alkanethiolate SAM matrices and imaged using STM, they exhibit bistable conductance switching, defined as ON when a molecule appears to protrude from the host matrix and OFF when the molecule is less protruding (or no longer visible within the host matrix). The apparent height of the molecule depends on (among other things) the thickness of the alkanethiolate SAM and the location of the molecule within the matrix.[18] The observed switching is due to a convolution of the physical height (change) of the molecule and the conductance of the molecule—substrate system.[15,16] Previously, we

showed that conductance switching was regulated by the packing of and interactions with the host matrix,[15,16,29,30] that the **OPE** molecules exhibited motion within the host matrix,[15,18] and that the switching and motion events occurred on time scales faster than those of STM imaging.[22] Several hypotheses for the observed conductance switching were tested by modifying the molecular design of the **OPE** moieties.[17] The only mechanism consistent with our and others' results is a change occurring at the substrate—molecule interface, which we posit to be a change in hybridization between the substrate and the molecule occurring mainly *via* molecular tilt.[15,16,25,29,30] Theoretical data likewise suggest that changes in the Au molecule bonding and the Au—Au arrangements strongly modify molecular conductance.[32−35] Here, molecular polarizability provides insight into the dynamics of the buried interface.

Molecular polarizabilities were measured locally and imaged using ACSTM in which two microwave frequency AC signals (in the range of 0.5−20 GHz), offset by a difference frequency (5 kHz), were combined with the DC bias voltage. The current used for the STM imaging feedback loop is dominated by the DC bias, with small contributions from the rectified AC signals. Applying two AC frequencies into our nonlinear tunneling junction enables us to measure the heterodyned AC signal at the difference frequency. We recorded the signals due to the applied microwave frequencies through the current preamplifier (bandwidth ~30 kHz).[1,36] To obtain microwave spectra and images, we used a lock-in amplifier referenced at the difference frequency to analyze the tunneling current, which carried the heterodyned microwave frequency information. The magnitude of the MDF signal is dependent on both the polarizability of the molecules and the STM tip-sample junction; therefore, the polarizability MDF images are, at present, relative measurements. We are able to compare the polarizabilities of molecules by measuring multicomponent monolayers and for switches by measuring the same molecules in the ON and OFF states. Thus, we are able to probe the electronic connection between the switch molecules and substrate (*i.e.*, the contacts[37−40]) by measuring polarizability (*vide supra*).

Figure 2 shows three different monolayers imaged using ACSTM and the corresponding schematic of each monolayer. These include fully saturated (no multiple bonds), partially saturated, and fully conjugated molecules, all of which form ordered monolayers. It also includes the simultaneously obtained polarizability maps. To compare the polarizabilities of different length alkanethiolate SAMs (shown schematically in Figure 2A), we formed a **C12** monolayer and vapor-annealed it with octanethiol, thereby forming domains of **C12** and **C8**.[41] The topographic (Figure 2B) and MDF polarizability (Figure 2C) images for a **C12/C8**-separated monolayer were recorded, and a small contrast was observed between the **C12** and **C8** molecules in the MDF signal. This small

contrast was expected from the microwave spectra recorded over the different length alkanethiolate chains since the calculated **C8** polarizability is ~76% that of **C12**.

When we imaged monolayers formed at room temperature from **1ATC9** molecules containing buried amide functionalities that are able to form hydrogen bonds, we observed two apparent height domains in the images, which we interpret as being due to different polar tilt angles of the **1ATC9** molecules (shown schematically in Figure 2D). This observation is consistent with surface infrared spectroscopy data that measured the possible tilt angles (between normal and tilted 18° from normal) to the surface to enable hydrogen bonding of the amide functionality.[42] When we imaged these monolayers, the apparent topographically less protruding (tilted) domains (Figure 2E) had a stronger MDF polarizability signal (Figure 2F) than the more protruding (normal to the surface) domains. Since the **1ATC9** molecules within the tilt domains are identical, and since their calculated gas-phase polarizabilities change very little when normal to the surface or tilted, we posit that the difference in the polarizabilities between the tilt domains is due to differences in the bonding at the molecule−surface interface.[44]

The monolayer packing of unfunctionalized **OPE** molecules has been described previously and is shown schematically in Figure 2G with the phenyl rings on neighboring molecules aligned perpendicular to one another.[43] From our polarizability calculations, we expect the unfunctionalized **OPE** molecules to have polarizabilities ~3−4 times that of **C12**, and when we measured these monolayers (Figure 2H), we found the experimental (relative) polarizabilities (Figure 2I) to be ~3 times that of **C12**.

We are unable to assemble complete, ordered monolayers of the nitro-functionalized **OPE** switch molecules due to their typical disorder and their limited stability in air.[44] However, using the insertion scheme detailed above, we *are* able to measure the polarizabilities and to follow the dynamics of these **OPE**-based single switch molecules. Time-lapse series of STM images recorded over fixed areas (500−1000 Å)² enabled us to record and to extract switching behavior and polarizabilities for each molecule in each frame (~5 min/frame) over several (8−18) hours. The first frame from one series of images is shown in Figure 3A,B, topography and MDF magnitude, respectively. Each inserted **OPE** molecule has been numerically labeled to correspond to the extracted frames in Figure 3C, which display the most dynamic 25 frames for each inserted molecule.

Since we are able to use MDF imaging to measure the polarizabilities of the nitro-functionalized **OPE** molecules, even at times when the molecules did not appear in the topographic images, we have used this as a means to locate switches in the OFF state and have at-
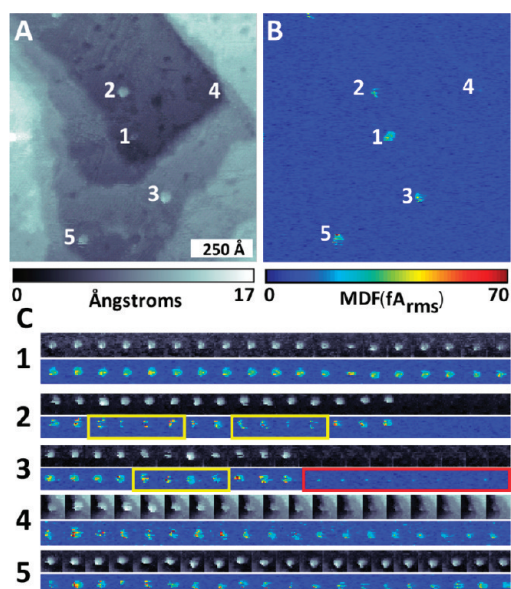
Figure 3. Simultaneously acquired (A) topographic and (B) MDF images of a dodecanethiolate SAM with inserted nitro-functionalized **OPE** molecular switches. A series of 200 images was acquired (5 min/frame, 30 s between frames). (C) Areas of 120 Å × 120 Å were extracted for each inserted molecular switch in each image. The numbers for the extracted series correspond to the labels in (A) and (B). The most dynamic 19 sequential frames are shown for each: **1** frames 4−22, **2** frames 93−112, **3** frames 88−107, **4** frames 4−21, and **5** frames 133−152. Molecules that were stable (did not switch or exhibit motion) had a constant MDF profile, as shown for **1**. Molecules that switched OFF showed fluctuations in the MDF images before they switched, highlighted by yellow boxes in **2** and **3**. Note that, in **3**, the **OPE** molecule still appeared in the MDF images after the molecule switched OFF (highlighted by red box in **3**). Molecules that exhibited motion within the SAM showed fluctuations in the MDF images as in **4** and **5**. Imaging conditions: V_{sample} = −1.0 V, I_{tunnel} = 2.0 pA, applied frequency = 2 GHz, difference frequency = 5 kHz, input power level = 10 dBm.

tempted to switch molecules deterministically using the electric field applied by the STM tip.[15] Our ability to switch these molecules was indicated (predicted) by instabilities in the MDF signal prior to applying the switching field. We and others have shown that substrate atom motion is important in switching.[22,45] Also note that we could deterministically switch **OPE** molecules from the ON to the OFF conductance state using the electric field applied by the STM tip without desorbing the switches, as shown in Figure 4. Controlled switching required different bias voltage magnitudes and tunneling gaps for different molecules, presumably due to the varied chemical environment created by defects in the surrounding monolayer matrix.[15,16,29,30] A more reliable method for controlled switching and stabilized conductance states has been demonstrated using the applied electric field and the stabilizing effects of hydrogen-bonding interactions between the active molecules and a specifically designed matrix;[29,30] however, for the purposes of this work, we have shown examples using only electric field.

Switching Molecule OFF:

Switching Molecule ON:
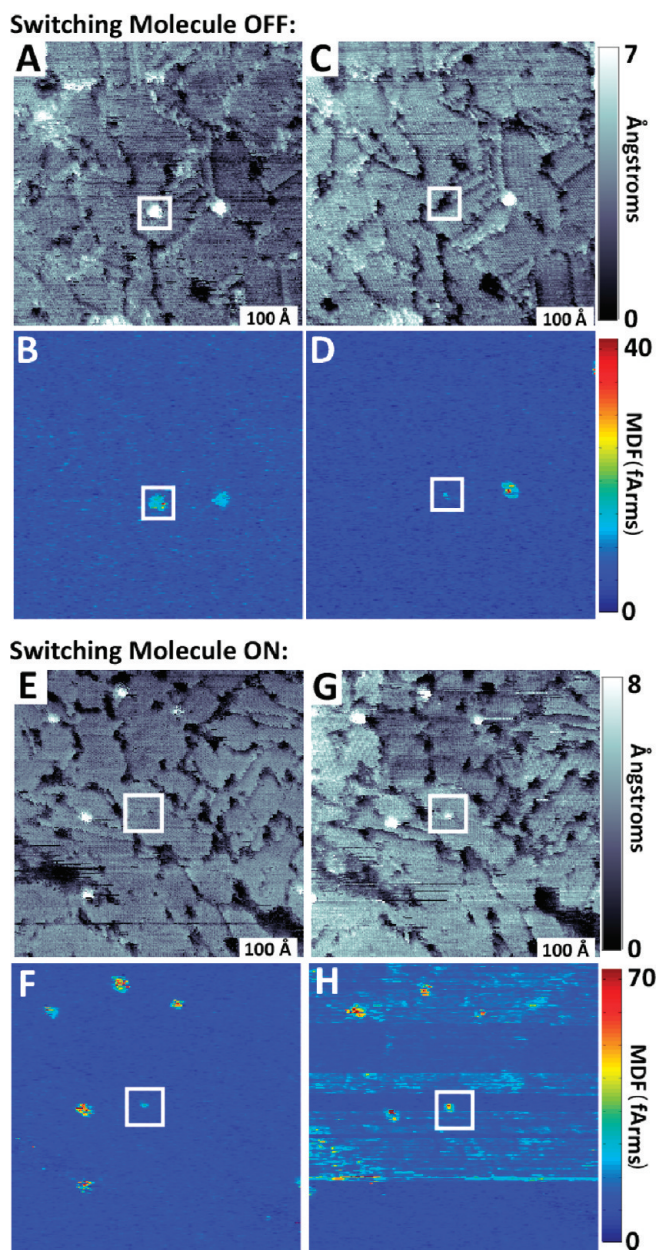
Figure 4. Controlled switching from the ON to the OFF (A−D) and from the OFF to the ON (E−H) conductance states for nitro-functionalized **OPE** molecules inserted into **C12** SAMs. (A,B) Simultaneously acquired topographic and MDF images in which two **OPE** molecules appear in the ON conductance state. After acquisition of these images, the STM tip was moved off center from the boxed molecule and the STM tip was moved 10 Å toward the sample five times (100 ms for each motion), followed by five voltage pulses from the tip (+2.0 V; 10 pA; 100 ms). We hypothesize that this loosened the SAM matrix[41] and allowed the molecule to switch from the ON to the OFF conductance states as shown in the subsequently acquired topographic (C) and MDF (D) images. The MDF image indicated that the molecule remained in the same location, even though it did not appear in the topographic image. (E,F) Simultaneously acquired topographic and MDF images where the boxed molecule does not appear in the topographic images but was imaged by the MDF. After three sequential images, each followed by moving the tip off center from the molecule and applying a voltage pulse (−1.0 V; 7 pA; 100 ms, final pulse, −1.5 V; 2 pA; 100 ms), the molecule switches to the ON conductance state as imaged in topography (G) and the simultaneous MDF image (H). Imaging conditions: $V_{sample} = -1.0$ V; $I_{tunnel} = 1.0$ pA (A−D); $I_{tunnel} = 2$ pA (E−H); applied frequency = 2 GHz; difference frequency = 5 kHz; input power level = 10 dBm.

TABLE 2. Comparison of Calculated and Experimental Polarizabilities for Nitro-Functionalized OPE Molecules[a]

		model parameters				experiment
	charge	neutral	neutral	anionic	anionic	
	geometry	neutral	anionic	neutral	anionic	ON
tilt	0° (normal)	4.61	4.86	**6.82**	5.96	**6.8 ± 3.6**
	30°	3.65	3.84	5.32	4.67	OFF
	45°	**2.69**	2.81	3.82	3.38	**2.5 ± 1.0**

[a]Polarizabilities were modeled for molecules in neutral and anionic states, with geometries optimized for either neutral or anionic states as indicated. Tilt indicates the modeled molecular tilt relative to the applied field. Polarizability is calculated in the direction of the field. Experimentally measured polarizabilities for nitro-**OPE** molecules in the ON and OFF states are compared with the closest theoretical matches: the anionic state with 0° tilt for molecules in the ON state, and the neutral state with 45° tilt for molecules in the OFF state (highlighted in bold).

Figure 4A−D shows a molecule switched from the ON to the OFF conductance states (boxed in Figure 4A,B), of topography and MDF magnitude, respectively.[46] The same area was imaged after switching (Figure 4C,D, topography and MDF image, respectively); the molecule's signature no longer appeared in the topographic image (it "disappears" into the matrix), but MDF imaging confirmed that the nitro-functionalized **OPE** switch was still present after the molecule was switched OFF. The ratios of the MDF signal for the ON and OFF nitro-functionalized OPE molecules to **C12** were 6.8 ± 3.6 and 2.5 ± 1.0, respectively. The ON state had a similar ratio to that calculated for the anionic nitro-functionalized OPE molecules oriented normal to the surface, while the OFF state ratio is most similar to the calculations for the neutral nitro-functionalized OPE molecule having a tilted geometry (Table 2). This large ratio between ON and OFF states indicates that the contribution to the measured polarizabilities of the molecules in the ON state due to the substrate electrons is substantial and at least equal to the contribution from the molecules' electrons.

Previously, we were typically limited to studying only molecules that appeared at some point in the ON conductance state during imaging, due to the difficulty in locating molecules continually in the OFF state in large topographic images.[15,16] With this method, we have the additional capability of locating, imaging, and measuring molecules that are in the OFF conductance state and do not appear in topography.

Figure 4E−H shows a molecule that was switched from the OFF conductance state to the ON state. In the initial topographic and MDF image (Figure 4E,F, topography and MDF image, respectively), the signature for the boxed molecule appeared in the MDF image and only as a slight protrusion in the topographic image. After several voltage pulses, the molecule switched to the ON conductance state (Figure 4G,H, topography and MDF image, respectively). This process is reversible. Note that the process also de-

stabilized the STM tip somewhat, leading to noisier images.[15,16]

CONCLUSIONS AND PROSPECTS

Using the ACSTM to obtain MDF images, we are able to measure single-molecule polarizabilities and to correlate them with calculated values. This enables us to relate the conductance state with the electronic coupling between the molecules and their contacts. As frustrated rotations partly determine this coupling, and electric fields can be used to actuate the switches, at higher applied microwave amplitudes, it may also be possible to determine the slew rates of the switches, which are expected to be in this range.[6,7,21,22]

The ability to measure conjugation and surface contact provides unique insights into the electronic interactions between single molecules and their immediate environment. The measurements described simultaneously and independently characterize surface topography and the substrate coupling at the buried interface. This is important because the behavior of conductive molecules depends strongly on their local coupling with macroscale electrodes, a fact that has hindered development in the field of molecular electronics.

Dielectric response measurements should also be possible at higher amplitude, enabling direct experimental evaluation of the relationship between individual dopant atom placement and nanoscale material properties in semiconductors.

Finally, we anticipate that these measurements may also enable chemical identification of local structural features in a macromolecule based on polarizability. Such a capability could represent a direct method for label-free, real-space structure determination from a single molecule.

EXPERIMENTAL AND THEORETICAL METHODS

Materials. The chemicals octanethiol, dodecanethiol, tetrahydrofuran (Sigma-Aldrich, St. Louis, MO), and 200-proof ethanol (Pharmco, Brookfield, CT) were used as received. Syntheses of compounds 4,4′-di(ethynylphenyl)-1-benzenethiol (**OPE**), (4,4′-di(ethynylphenyl)-2′-nitro-1-benzenethiol) (**nitro-OPE**), and 3-mercapto-*N*-nonylpropionamide (**1ATC9**) have been described previously.[47,48]

Sample Preparation. The SAM matrices were formed on Au{111} on mica substrates (Agilent Technologies), which were annealed with a hydrogen flame immediately prior to film preparation. Matrices studied for polarizability were deposited from 1 mM ethanolic solutions of the matrix molecule for 24−48 h. Monolayers used for subsequent insertion were deposited from 1 mM solutions of dodecanethiol in ethanol for 5 min. This short adsorption time forms a less ordered matrix and enables more switching of the inserted molecules.[15] The samples were rinsed with neat ethanol and blown dry with nitrogen. Insertion of **OPE** was performed under a nitrogen environment by placing the preformed SAMs into 0.1 mM solutions of 4,4′-di(ethynylphenyl)-1-benzenethiol in tetrahydrofuran for 1 min. The samples were rinsed with ethanol after insertion and dried with nitrogen prior to imaging.

STM Measurements. All STM measurements were performed in a custom Besocke-style STM under ambient conditions. The STM is equipped with two microwave frequency generators (Hewlett-Packard, 8263B), which are used to add a sinusoidal bias modulation at microwave frequencies from 0.5 to 20 GHz.[2−5] The applied frequencies are offset by a small difference frequency (typically 5 kHz), mixed (Hewlett-Packard, 87302C), and split through a directional coupler (Hewlett-Packard, 87300C). One output of the directional coupler is combined with the DC bias voltage using a bias tee (Hewlett-Packard, 11612A) and used to apply a bias to the STM tip. The other output first passes through a detector diode (Narda, 4503A), then to a low-pass filter (Frequency Devices, ASC-50), which amplifies the difference signal before passing it to the lock-in amplifier (Stanford Research Systems, SR850) as a reference. Microwave difference signals applied to the sample through the STM tip first passed through the current preamplifier (Axon CV-4, bandwidth 30 kHz) and were detected at the lock-in amplifier.

Theory. Polarizability values were calculated using density functional theory (DFT) with the B3LYP functional and a 6-31^{++}G** basis set.[19] These include calculations for molecules aligned normal to the surface and in tilted conformations and for both anionic and neutral states of the nitro-functionalized **OPE** molecules. Calculations are performed for molecules in the gas phase, with no explicit contribution from substrate atoms.

REFERENCES AND NOTES

1. Bumm, L. A.; Arnold, J. J.; Cygan, M. T.; Dunbar, T. D.; Burgin, T. P.; Jones, L.; Allara, D. L.; Tour, J. M.; Weiss, P. S. Are Single Molecular Wires Conducting? *Science* **1996**, *271*, 1705–1707.
2. Stranick, S. J.; Weiss, P. S. A Versatile Microwave-Frequency-Compatible Scanning Tunneling Microscope. *Rev. Sci. Instrum.* **1993**, *64*, 1232–1234.
3. Stranick, S. J.; Weiss, P. S. Alternating-Current Scanning-Tunneling-Microscopy and Nonlinear Spectroscopy. *J. Phys. Chem.* **1994**, *98*, 1762–1764.
4. Stranick, S. J.; Weiss, P. S. A Tunable Microwave Frequency Alternating-Current Scanning Tunneling Microscope. *Rev. Sci. Instrum.* **1994**, *65*, 918–921.
5. Bumm, L. A.; Weiss, P. S. Small Cavity Nonresonant Tunable Microwave-Frequency Alternating-Current Scanning Tunneling Microscope. *Rev. Sci. Instrum.* **1995**, *66*, 4140–4145.
6. Moore, A. M.; Weiss, P. S. Functional and Spectroscopic Measurements with Scanning Tunneling Microscopy. *Annu. Rev. Anal. Chem.* **2008**, *1*, 857–882.
7. Weiss, P. S. Functional Molecules and Assemblies in Controlled Environments: Formation and Measurements. *Acc. Chem. Res.* **2008**, *41*, 1772–1781.
8. Han, P.; Kurland, A. R.; Giordano, A. N.; Nanayakkara, S. U.; Blake, M. M.; Pochas, C. M.; Weiss, P. S. Heads and Tails: Simultaneous Exposed and Buried Interface Imaging of Monolayers. *ACS Nano* **2009**, *3*, 3115–3121.
9. Giepmans, B. N. G.; Adams, S. R.; Ellisman, M. H.; Tsien, R. Y. The Fluorescent Toolbox for Assessing Protein Location and Function. *Science* **2006**, *312*, 217–224.
10. Pavani, S. R. P.; Thompson, M. A.; Biteen, J. S.; Lord, S. J.; Liu, N.; Twieg, R. J.; Piestun, R.; Moerner, W. E. Three-Dimensional, Single-Molecule Fluorescence Imaging beyond the Diffraction Limit by Using a Double-Helix Point Spread Function. *Proc. Natl. Acad. Sci. U.S.A.* **2009**, *106*, 2995–2999.
11. Hinterdorfer, P.; Dufrene, Y. F. Detection and Localization of Single Molecular Recognition Events Using Atomic Force Microscopy. *Nat. Methods* **2006**, *3*, 347–355.

12. Stranick, S. J.; Bumm, L. A.; Kamna, M. M.; Weiss, P. S. Linear and Nonlinear Spectroscopy with the Tunable AC Scanning Tunneling Microscope. In *Photons and Local Probes*; Marti, O., Muller, R., Eds.; NATO ASI Series E: Applied Sciences 300, Kluwer Academic: Dordrecht, The Netherlands, 1995; p 221.

13. Cyr, D. M.; Venkataraman, B.; Flynn, G. W.; Black, A.; Whitesides, G. M. Functional Group Identification in Scanning Tunneling Microscopy of Molecular Adsorbates. *J. Phys. Chem.* **1996**, *100*, 13747–13759.

14. Cyr, D. M.; Venkataraman, B.; Flynn, G. W. STM Investigations of Organic Molecules Physisorbed at the Liquid−Solid Interface. *Chem. Mater.* **1996**, *8*, 1600–1615.

15. Donhauser, Z. J.; Mantooth, B. A.; Kelly, K. F.; Bumm, L. A.; Monnell, J. D.; Stapleton, J. J.; Price, D. W.; Rawlett, A. M.; Allara, D. L.; Tour, J. M. Conductance Switching in Single Molecules through Conformational Changes. *Science* **2001**, *292*, 2303–2307.

16. Donhauser, Z. J.; Mantooth, B. A.; Pearl, T. P.; Kelly, K. F.; Nanayakkara, S. U.; Weiss, P. S. Matrix-Mediated Control of Stochastic Single Molecule Conductance Switching. *Jpn. J. Appl. Phys.* **2002**, *41*, 4871–4877.

17. Moore, A. M.; Dameron, A. A.; Mantooth, B. A.; Smith, R. K.; Fuchs, D. J.; Ciszek, J. W.; Maya, F.; Yao, Y. X.; Tour, J. M.; Weiss, P. S. Molecular Engineering and Measurements To Test Hypothesized Mechanisms in Single Molecule Conductance Switching. *J. Am. Chem. Soc.* **2006**, *128*, 1959–1967.

18. Moore, A. M.; Mantooth, B. A.; Donhauser, Z. J.; Maya, F.; Price, D. W.; Yao, Y. X.; Tour, J. M.; Weiss, P. S. Cross-Step Place-Exchange of Oligo(phenylene-ethynylene) Molecules. *Nano Lett.* **2005**, *5*, 2292–2297.

19. Shao, Y.; Molnar, L. F.; Jung, Y.; Kussmann, J.; Ochsenfeld, C.; Brown, S. T.; Gilbert, A. T. B.; Slipchenko, L. V.; Levchenko, S. V.; O'Neill, D. P.; *et al.* Advances in Methods and Algorithms in a Modern Quantum Chemistry Program Package. *Phys. Chem. Chem. Phys.* **2006**, *8*, 3172–3191.

20. Deutsch, D.; Natan, A.; Shapira, Y.; Kronik, L. Electrostatic Properties of Adsorbed Polar Molecules: Opposite Behavior of a Single Molecule and a Molecular Monolayer. *J. Am. Chem. Soc.* **2007**, *129*, 2989–2997.

21. Mantooth, B. A.; Weiss, P. S. Fabrication, Assembly, and Characterization of Molecular Electronic Components. *Proc. IEEE* **2003**, *91*, 1785–1802.

22. Moore, A. M.; Mantooth, B. A.; Donhauser, Z. J.; Yao, Y. X.; Tour, J. M.; Weiss, P. S. Real-Time Measurements of Conductance Switching and Motion of Single Oligo(phenylene ethynylene) Molecules. *J. Am. Chem. Soc.* **2007**, *129*, 10352–10353.

23. Chen, J.; Reed, M. A.; Rawlett, A. M.; Tour, J. M. Large On−Off Ratios and Negative Differential Resistance in a Molecular Electronic Device. *Science* **1999**, *286*, 1550–1552.

24. Reichert, J.; Ochs, R.; Beckmann, D.; Weber, H. B.; Mayor, M.; von Lohneysen, H. Driving Current through Single Organic Molecules. *Phys. Rev. Lett.* **2002**, *88*, 176804.

25. Ramachandran, G. K.; Hopson, T. J.; Rawlett, A. M.; Nagahara, L. A.; Primak, A.; Lindsay, S. M. A Bond-Fluctuation Mechanism for Stochastic Switching in Wired Molecules. *Science* **2003**, *300*, 1413–1416.

26. Kushmerick, J. G.; Naciri, J.; Yang, J. C.; Shashidhar, R. Conductance Scaling of Molecular Wires in Parallel. *Nano Lett.* **2003**, *3*, 897–900.

27. Cai, L. T.; Skulason, H.; Kushmerick, J. G.; Pollack, S. K.; Naciri, J.; Shashidhar, R.; Allara, D. L.; Mallouk, T. E.; Mayer, T. S. Nanowire-Based Molecular Monolayer Junctions: Synthesis, Assembly, and Electrical Characterization. *J. Phys. Chem. B* **2004**, *108*, 2827–2832.

28. Selzer, Y.; Cabassi, M. A.; Mayer, T. S.; Allara, D. L. Thermally Activated Conduction in Molecular Junctions. *J. Am. Chem. Soc.* **2004**, *126*, 4052–4053.

29. Lewis, P. A.; Inman, C. E.; Yao, Y. X.; Tour, J. M.; Hutchison, J. E.; Weiss, P. S. Mediating Stochastic Switching of Single Molecules Using Chemical Functionality. *J. Am. Chem. Soc.* **2004**, *126*, 12214–12215.

30. Lewis, P. A.; Inman, C. E.; Maya, F.; Tour, J. M.; Hutchison, J. E.; Weiss, P. S. Molecular Engineering of the Polarity and Interactions of Molecular Electronic Switches. *J. Am. Chem. Soc.* **2005**, *127*, 17421–17426.

31. Meded, V.; Bagrets, A.; Arnold, A.; Evers, F. Molecular Switch Controlled by Pulsed Bias Voltages. *Small* **2009**, *5*, 2218–2223.

32. Di Ventra, M.; Pantelides, S. T.; Lang, N. D. First-Principles Calculation of Transport Properties of a Molecular Device. *Phys. Rev. Lett.* **2000**, *84*, 979–982.

33. Basch, H.; Cohen, R.; Ratner, M. A. Interface Geometry and Molecular Junction Conductance: Geometric Fluctuation and Stochastic Switching. *Nano Lett.* **2005**, *5*, 1668–1675.

34. Andrews, D. Q.; Van Duyne, R. P.; Ratner, M. A. Stochastic Modulation in Molecular Electronic Transport Junctions: Molecular Dynamics Coupled with Charge Transport Calculations. *Nano Lett.* **2008**, *8*, 1120–1126.

35. Kristensen, I. S.; Mowbray, D. J.; Thygesen, K. S.; Jacobsen, K. W. Comparative Study of Anchoring Groups for Molecular Electronics: Structure and Conductance of Au−S−Au and Au−NH_2−Au Junctions. *J. Phys.: Condens. Matter* **2008**, *20*, 374101.

36. Miller, R. C. Optical Second Harmonic Generation in Piezoelectric Crystals. *Appl. Phys. Lett.* **1964**, *5*, 17–19.

37. Beebe, J. M.; Engelkes, V. B.; Miller, L. L.; Frisbie, C. D. Contact Resistance in Metal−Molecule−Metal Junctions Based on Aliphatic SAMs: Effects of Surface Linker and Metal Work Function. *J. Am. Chem. Soc.* **2002**, *124*, 11268–11269.

38. Monnell, J. D.; Stapleton, J. J.; Dirk, S. M.; Reinerth, W. A.; Tour, J. M.; Allara, D. L.; Weiss, P. S. Relative Conductances of Alkaneselenolate and Alkanethiolate Monolayers on Au{111}. *J. Phys. Chem. B* **2005**, *109*, 20343–20349.

39. Chen, F.; Hihath, J.; Huang, Z. F.; Li, X. L.; Tao, N. J. Measurement of Single-Molecule Conductance. *Annu. Rev. Phys. Chem.* **2007**, *58*, 535–564.

40. Bumm, L. A. Measuring Molecular Junctions: What Is the Standard? *ACS Nano* **2008**, *2*, 403–407.

41. Donhauser, Z. J.; Price, D. W.; Tour, J. M.; Weiss, P. S. Control of Alkanethiolate Monolayer Structure Using Vapor-Phase Annealing. *J. Am. Chem. Soc.* **2003**, *125*, 11462–11463.

42. Tam-Chang, S. W.; Biebuyck, H. A.; Whitesides, G. M.; Jeon, N.; Nuzzo, R. G. Self-Assembled Monolayers on Gold Generated from Alkanethiols with the Structure $RNHCOCH_2SH$. *Langmuir* **1995**, *11*, 4371–4382.

43. Yang, G. H.; Qian, Y. L.; Engtrakul, C.; Sita, L. R.; Liu, G. Y. Arenethiols Form Ordered and Incommensurate Self-Assembled Monolayers on Au(111) Surfaces. *J. Phys. Chem. B* **2000**, *104*, 9059–9062.

44. Richter, L. J.; Yang, C. S. C.; Wilson, P. T.; Hacker, C. A.; van Zee, R. D.; Stapleton, J. J.; Allara, D. L. Optical Characterization of Oligo(phenylene-ethynylene) Self-Assembled Monolayers on Gold. *J. Phys. Chem. B* **2004**, *108*, 12547–12559.

45. Yu, M.; Bovet, N.; Satterley, C. J.; Bengio, S.; Lovelock, K. R. J.; Milligan, P. K.; Jones, R. G.; Woodruff, D. P.; Dhanak, V. True Nature of an Archetypal Self-Assembly System: Mobile Au-Thiolate Species on Au(111). *Phys. Rev. Lett.* **2006**, *97*, 166102.

46. Yang, G. H.; Liu, G. Y. New Insights for Self-Assembled Monolayers of Organothiols on Au(111) Revealed by Scanning Tunneling Microscopy. *J. Phys. Chem. B* **2003**, *107*, 8746–8759.

47. Tour, J. M.; Rawlett, A. M.; Kozaki, M.; Yao, Y. X.; Jagessar, R. C.; Dirk, S. M.; Price, D. W.; Reed, M. A.; Zhou, C. W.; Chen, J. Synthesis and Preliminary Testing of Molecular Wires and Devices. *Chem.—Eur. J.* **2001**, *7*, 5118–5134.

48. Clegg, R. S.; Reed, S. M.; Hutchison, J. E. Self-Assembled Monolayers Stabilized by Three-Dimensional Networks of Hydrogen Bonds. *J. Am. Chem. Soc.* **1998**, *120*, 2486–2487.